Revised Manuscript (clean for typesetting) Click here to view linked References

Role of Granular Activated Carbon's Physical Properties and Surface Chemistry in Sustaining Biological Activated Carbon Performance

Han Chen[†,‡], Junling Wang[†], Lei Xu[‡*], Peng Zhou[‡], Nigel J. D. Graham [§], Wenzheng Yu[‡*]

[†] College of Environmental and Energy Engineering, Beijing University of Civil Engineering & Architecture, Beijing 100044, China

[‡] Key Laboratory of Drinking Water Science and Technology, Research Centre for Eco-Environmental Sciences, Chinese Academy of Sciences, Beijing 100086, China

[§] Department of Civil and Environmental Engineering, Imperial College London, South Kensington Campus, London SW7 2AZ, United Kingdom

Abstract: The removal of natural organic matter (NOM) through biofiltration can be significantly influenced by the diversity of acclimated microbes on the substrate surface. In this study, three types of granular activated carbon (GAC), each with different surface functional group distributions, were selected as substrates for biofiltration to explore their effects on microbial and NOM removal in surface water. The results showed that GAC with a higher percentage of carboxyl group achieved better NOM removal efficiency during approximately one year of continuous operation (83.6 ± 1.4%). Using Fourier-transform ion cyclotron resonance mass spectrometry (FT-ICR-MS), it was found that coal-based GAC(C-GAC) was more effective at removing biorefractory compounds of NOM, including 42%, 47%, and 59% more lignin, tannins, and condensed aromatic hydrocarbons, respectively. Microbial sequencing analyses revealed that physical and chemical properties of C-GAC favored the acclimation of species involved in the biodegradation of humic substances, such as the family *Rhodocyclaceae* and the genus *Desulfosporosinus*. More importantly, microbial interactions and metabolism (related to biodegradation) were found to be strongly influenced by the surface carboxyl group and pore size distribution of GAC, with the influence of surface carboxyl group being particularly critical. This study provides

valuable insights into how the physicochemical properties of GAC synergistically govern microbial community dynamics and DOM removal efficiency, laying a foundation for enhancing the performance of biofilters in future water purification and reuse applications.

Keywords: Carboxyl group; Natural organic matter; Biodegradation; Microbial diversity; Metabolism pathways

Introduction

In recent years, the intensification of urbanization and agricultural activities has led to increased water demand and a heightened risk of water pollution, thereby restricting the safe use of water resources. Research indicates that water pollution exacerbates water scarcity in global watersheds, and under worst-case scenarios, up to 3 billion people may face severe water shortages by 2050 (Jones et al., 2024; Wang et al., 2024). Consequently, the recycling and reuse of water resources, particularly for agricultural irrigation and drinking water, is an increasingly important strategy for sustainable development (Christou et al., 2024; Shah et al., 2024). To facilitate the reuse of water resources, it is essential to eliminate contaminants and NOM. Among the range of current water treatment technologies, biological filtration is not only recognized for its cost-effectiveness but also for its operability, robustness, and long service life, thus playing a significant role in water recycling and reuse processes.

Biological activated carbon (BAC) is widely utilized in biological filtration systems due to its superior characteristics, combining substance adsorption, particle separation and biomass support. Compared to conventional filter media, such as sand and zeolite, activated carbon (AC) boasts a substantially greater specific surface area and a wealth of surface functional groups. These advantages enable AC to selectively adsorb organic micro-pollutants and NOM (Karanfil et al., 1996; Karanfil et al., 1999) while also providing a beneficial surface morphology for microbial colonization (Lu et al., 2021).

Studies have demonstrated that the effective particle size of GAC influences the biomass of key microbial species, while surface functional groups significantly impact the adhesion of microorganisms to the carbon surface (Lu et al., 2022). The operation of biofiltration can be categorized into three primary stages: physical adsorption, a combination of physical adsorption and biodegradation, and biodegradation processes. Over the long term, biodegradation provides the principal mechanism for pollutant removal, ensuring a high efficiency and stability within the biofiltration process.

The biodegradability in biofiltration systems is influenced by several factors, including the biomass, community structure, and growth rate of microbial populations (Oh et al., 2018; Wang et al., 1995), and research has indicated that community structure may be a primary determinant of biodegradability (Lu et al., 2022). In addition, environmental conditions (like DOM characteristics, dissolved oxygen, etc.) can significantly impact microbial community structures, thereby indirectly affecting the effluent quality of the biofiltration process (Huang et al., 2024; Xu et al., 2024). Dissolved oxygen, as one of the environmental factors, acts as an electron acceptor in the microbial electron transfer process in the water column, and its concentration not only affects the transfer rate, but also influences the diversity of microorganisms, which in turn affects the system performance.(Han et al., 2013; Liu et al., 2023a; Liu et al., 2023b). Moreover, the characteristics of NOM have been shown to influence microbial metabolism, leading to alterations in microbial community structures (Blair et al., 2024; Gerrity et al., 2018; Siembida-Losch et al., 2015). Although several studies have reported correlations between GAC characteristics and microbial communities, comprehensive research integrating GAC properties, microbial community dynamics, and NOM characteristics is still lacking. The interactions among these three aspects remain poorly understood.

Following long-term operation of biofiltration systems, the degradation pathways and end products generated from NOM are closely related to, and can be influenced by, the composition of the microbial community. Microbial diversity enhances the metabolic capacity of these communities, fostering synergistic interactions among microbes and

84 resulting in functionally complementary communities(Wang et al., 2023). Within a
85 community, certain metabolic functions are carried out collectively by multiple species.
86 The absence of any single species does not impair these functions, thereby reducing
87 dependence on individual species and enhancing overall system stability (Chen et al.,
88 2024; Wagg et al., 2019). In the context of biodegradation of NOM, the complex
89 characteristics of DOM influences the degradation capacity of the microbial community
90 (Dal Bello et al., 2021; FOG, 1988). Consequently, the composition and decomposition
91 processes of NOM are intricately linked to microbial degradation mechanisms (Antony
92 et al., 2017; Bianco et al., 2019). However, research and knowledge on the
93 intermolecular transformations of NOM induced by microbial variations, particularly
94 as influenced by differences in the physical and chemical properties of GAC, remains
95 limited. This gap highlights the need for further investigation to enhance our
96 understanding of NOM degradation in BAC filters.

97 This study investigates the synergistic effects of various types of GAC, differing in
98 specific surface area and the distribution of surface functional groups, used as substrates
99 in BAC filters. Specifically, the research focuses on the impact of GAC
100 physicochemical properties on microbial diversity and the corresponding
101 interconnectivity between microbes and NOM. The findings provide a comprehensive
102 evaluation of the relationship between GAC properties, microbial diversity, and
103 biofiltration performance in terms of NOM removal, thereby contributing significantly
104 to the potential applications of BAC filters in water recycling and reuse scenarios.

105

106 **Materials and methods**

107 **2.1. Setup and operation of BAC filters**

108 This study utilized continuous upflow bench-scale BAC filtration systems to treat
109 surface water sourced from an artificial lake (Olympic Park, Beijing, China) that flows
110 into a natural river; this water was the ‘raw water’ for the filter tests. The BAC filtration

system comprised circular Plexiglas columns with a diameter of 50 mm and a height of 500 mm, utilizing three types of GAC as filter media: coal-based GAC (C-GAC), bamboo-based GAC (B-GAC), and coconut shell-based GAC (CS-GAC), with an average carbon granule size of 3-5 mm. The approximate height of the media in each column was 475 mm, resulting in a net liquid volume of approximately 350 mL (bed porosity ~0.38). Each column featured three sampling ports located at distances of 160, 320 and 475 mm from the bottom, designated as 'Bot', 'Mid' and 'Top' (the order corresponding to the direction of flow).

Prior to the start of the filtration tests, the filters were inoculated with soil microbes sourced from the lake bank, and raw water was continuously fed to the filter systems from a common influent tank. The operation was divided into three stages, each characterized by a progressively decreasing hydraulic retention time (HRT; based on total bed height and porosity): 24 h (Days 1-250), 12 h (Days 251-317), and 6 h (Days 318-357). This allowed us to investigate the effects of HRT on DOM removal performance across the three systems.

2.2. Characterizations of GAC

For BET (Brunner-Emmet-Teller) measurements, GAC samples were subjected to standardized degassing procedures using a degassing station (Mike; USA) at 300 °C under vacuum for 3 h. Subsequently, nitrogen adsorption and desorption tests were conducted using a fully automated specific surface area analyzer (Micromeritics APSP 2460; USA) at 77 K with liquid nitrogen. The total specific surface area, pore volume, micropore volume, and micropore size distributions of the samples were determined using the BET, t-plot, BJH (Barrett-Joyner-Halenda), and HK (Horvath-Kawazoe) methods, respectively. The electrical resistivity of GAC was determined using a multimeter (VICTOR VC890D) with two polished copper sheets serving as clip electrodes (electrode resistance < 0.1Ω). The average GAC granule diameter for each GAC type was determined by vernier caliper measurements conducted on 20 to 30 granules to ensure representative results.

The Boehm method was employed to quantify the proportion of surface functional groups, specifically carboxyl, lactonic, and phenolic hydroxyl groups, on GAC surfaces (Goertzen et al., 2010; Oickle et al., 2010). X-ray photoelectron spectroscopy (XPS; PHI Quantera II, ULVAC, Japan) was used to analyze the chemical compositions and oxidation states of elements on freeze-dried samples, utilizing a Thermo Escalab 250 electron spectrometer with 150 W Al-Kα radiation.

Kinetic batch adsorption tests were conducted to model the adsorption by pseudo first-order and pseudo second-order kinetic reaction equations, enabling an understanding of adsorption rates and capacities for each GAC type. These tests also facilitated a comparison between physical and chemical adsorption processes. Details of the analysis are provided in the supplementary information (SI, Text S1).

2.3. Speciation and quantification of NOM

Water samples were filtered through 0.45-μm syringe filters prior to all analyses. Dissolved organic carbon (DOC) concentrations were quantified using a total organic carbon analyzer (TOC-Vwp, Shimadzu, Japan). The UV-visible absorption spectra were obtained via UV-visible spectroscopy (UV-2600, Shimadzu, Japan). The fluorescence characteristics of NOM in the water samples were analyzed using three-dimensional excitation-emission matrix (EEM) fluorescence spectroscopy. The EEM spectrum was divided into five regions (I-V) based on the properties of the fluorescent substances, and the fluorescence intensity of each region was quantified using fluorescence region integration (FRI) (SI, Table S1). Additionally, the common fluorescent components in the water samples were analyzed using parallel factor analysis (PARAFAC). Detailed procedures regarding the pre-processing of EEM data for the FRI and PARAFAC are provided in the supplementary information (Text S2). The molecular weight distribution of NOM was determined using a high-performance liquid chromatography (HPLC) system (Waters, USA), coupled with a size exclusion chromatography (SEC) column. The details of SEC measurements are provided in the supplementary information (Text S3). Freeze-dried water samples were also analyzed

using Fourier Transform Infrared Spectroscopy (FTIR, Spectrum TWO, PerkinElmer, USA).

To further investigate changes in NOM at the molecular level, solid-phase extraction (SPE) was conducted using an Agilent Bond Elute PPL column, followed by FT-ICR-MS analysis using a Bruker SolariX FT-ICR-MS instrument fitted with a 15.0 T superconducting magnet and an electrospray ionization (ESI) source. The weight-mean double bond equivalence (DBE), nominal oxidation state of carbon (NOSC), and modified aromaticity index (AImod) of the molecules were calculated, and the number of aliphatic substances was quantified. Detailed procedures regarding SPE, FT-ICR-MS measurements, and related calculations are provided in the supplementary information (SI, Text S4).

2.4. Characterization of biofilms on BAC

At the end of the period of operation, 40 g of BAC was removed from the middle sampling port of each biofilter and stored in sterile centrifuge tubes at -20 °C until further processing, which included measuring the content of extracellular polymeric substances (EPS) and extracting DNA for 16S rRNA analysis. Sampling from the middle section helps avoid the effects of excessive DOM at the bottom, which can increase community complexity, as well as the loss of important species at the top due to insufficient DOM. EPS were extracted using phosphate-buffered saline (PBS) according to the method described previously (D'Abzac et al., 2010). The concentrations of polysaccharides and proteins were quantified using UV-Vis spectrophotometry, with triplicate measurements conducted (SI, Text S5). For high-throughput sequencing, the obtained results were filtered and denoised, and the sequence counts for each sample were normalized to a uniform depth of 28,673 sequences. The composition and diversity of the microbial communities were processed and analyzed through the Majorbio Cloud Platform. Microbial co-occurrence networks were constructed using R and visualized with Gephi version 0.10.1. The raw sequencing data were deposited in the Sequence Read Archive database of the National Center for

Biotechnology Information (NCBI) under accession number PRJNA1202848. Further details are provided in the supplementary information (SI, Text S6). To gain further insights into the relationships among microbial diversity, the physical and chemical properties of GAC, and NOM removal efficiency, Mantel tests and Partial Least Squares Path Modeling (PLS-PM) were conducted using R.

The electrochemical properties of BAC in each biofilter were examined using a three-electrode system, with Ag/AgCl (saturated KCl) serving as the reference electrode, platinum (Pt) as the counter electrode, and BAC is fixed by the working electrode clamp as the working electrode. For cyclic voltammetry (CV) measurements (scan rate: 0.05 V/s, potential window: -1.0 to 1.0 V, and six scan segments), the effluent from the biofilter was utilized as the electrolyte, supplemented with 0.5 M anhydrous sodium sulfate to enhance electrolyte conductivity. Electrochemical impedance spectroscopy (EIS) measurements were conducted under open-circuit conditions, covering a frequency range of 10^{-1} to 10^{6} Hz, and the obtained curves were fitted using ZView software (version 2.9, Scribner Associates, Inc.). At least ten BAC granules of similar size from each system were selected for electrochemical measurements to ensure the reproducibility of the results. Error bars in all figures represent the standard deviations of values obtained from replicate measurements.

Results and discussion

Physical and chemical characterizations of GAC

The adsorption capacity of GAC is influenced by multiple factors, including its physical and chemical properties, as well as the surrounding environmental conditions (Karanfil and Kilduff, 1999; Lu et al., 2022). Based on BET measurements, the pores of GAC can be categorized into three types according to their size: micropores (diameter < 2 nm), mesopores (2 nm < diameter < 50 nm), and macropores (diameter > 50 nm). Among the three types of GAC studied, B-GAC exhibited the highest micropore

volume (4.71 $cm^3/(g•nm)$), whereas C-GAC displayed the lowest micropore volume (3.45 $cm^3/(g•nm)$). However, C-GAC had the highest volume of mesopores (1.84 $cm^3/(g•nm)$), compared to B-GAC (0.7 $cm^3/(g•nm)$) and CS-GAC (0.6 $cm^3/(g•nm)$) (Figure 1A). It is well-established that a greater volume of micropores of GAC contributes to a larger specific surface area overall, which is consistent with the observed results, indicating that B-GAC possessed the largest specific surface area (1029.98 m^2/g), followed by CS-GAC (872.73 m^2/g) and C-GAC (870.56 m^2/g) (Figure 1C). Previous studies have also demonstrated that B-GAC has a larger specific surface area and higher adsorption capacity (e.g. organic pollutants, heavy metals, and phenols) compared to both C-GAC and CS-GAC (Hashim et al., 2022; Kim et al., 2009; Nyika and Dinka, 2022). This enhanced performance is primarily attributed to the pronounced pore structure formed from bamboo fibers during the carbonization process (Cheng et al., 2023). Additionally, compared to B-GAC (16.3%) and CS-GAC (15.7%), C-GAC (31.9%) exhibits the highest mesopore distribution ratio, which may facilitate electron transfer by enhancing connectivity between carbon particles(Li et al., 2022). Because the presence of a mesoporous structure facilitates stronger interconnections among carbon particles, promoting the formation of continuous conductive pathways and effectively minimizing interfacial contact resistance (Huang et al., 2019; Zhai et al., 2011).

Figure 1

The distribution of surface functional groups in GAC was examined using the Boehm-titration method (Figure 1D). The results indicated that C-GAC had a higher concentration of carboxyl group (-COOH) at 0.098 ± 0.004 (mM/(L·g)), compared to B-GAC at 0.058 ± 0.013 (mM/(L·g)) and CS-GAC at 0.032 ± 0.010 (mM/ (L·g)) (calculated based on the weight of sample tested). This finding is consistent with the O1s and C1s results obtained from the corresponding XPS measurements (Figure 1E). In the N1s spectra, C-GAC exhibited a higher percentage of pyrrole and pyridine nitrogen groups (33.22%) compared to B-GAC (10.59%) and CS-GAC (32.22%).

Previous studies have indicated that the presence of hydrophilic group(carboxyl group and phenolic hydroxyl group) and nitrogen heteroatoms can improve the hydrophilic characteristics of GAC, thereby reducing solid/liquid interface resistance (Yuksel and Karakehya, 2024). Furthermore, condensed nitrogen structures have been shown to enhance the electronic conductivity of carbon materials (Cordero-Lanzac et al., 2018). This observation is supported by measurements of the electrical conductivity of GAC, which revealed that C-GAC (0.82 ± 0.24 Ω) exhibited the lowest electrical resistance when compared to B-GAC (1.00 ± 0.20 Ω) and CS-GAC (1.39 ± 0.3 Ω). Moreover, the results are consistent with the pattern of mesopore distribution, further demonstrating the critical role of pore size distribution. The more abundant the carboxyl groups on the GAC surface, the lower the electrical resistance exhibits. In contrast, the phenolic hydroxyl groups show an opposite trend, where higher content leads to increased electrical resistance. Interestingly, although CS-GAC (32.22%) contains a higher concentration of nitrogen heteroatoms than B-GAC (10.59%), its resistance (1.39 ± 0.3 Ω) was much higher than B-GAC (1.00 ± 0.20 Ω). This suggests that the effect of N-hybridized atoms is also secondary, probably because the N element in GAC is much lower than the C, H, and O elements, and its resistance was greater than that of B-GAC, highlighting the significance of carboxyl group and pore size distribution in influencing the electrical conductivity of GAC (Gryglewicz et al., 2005; Yuksel and Karakehya, 2024).

Variation of NOM removal during the long-term operation

As illustrated in Figure 2A (and SI, Figure S3), the three systems utilizing different types of GAC exhibited varying capabilities in removing NOM over the long-term operation. During the initial period of the operation (the first 50 days), no significant differences were observed in the solutions from the top and mid locations (SI, Figure S2), likely because the GAC had not yet reached adsorption saturation (physical adsorption stage). However, in the bottom location, CS-GAC demonstrated the lowest DOC removal compared to both B-GAC and C-GAC, which aligns with the results of

the adsorption kinetics experiments (Figure S4). During the second phase (225–257 days), significant differences emerged in effluent quality among the three systems, with this trend becoming more pronounced toward the end of the phase. Analysis showed that the DOM removal rates of the three systems at the end of this phase were comparable to those at the beginning. The primary reason was the summer season, during which large algal blooms caused a sudden increase in dissolved organic matter (DOM) in the raw water, thereby elevating the DOM concentration in the effluent. As the stage where adsorption saturation occurs and biodegradation plays a dominant role (318-357 days), the NOM removal efficiency in the top location decreased to approximately 60% for both B-GAC and CS-GAC, while the C-GAC maintained a NOM removal efficiency of around 90%. It was investigated that C-GAC improved the removal of DOM by at least about 30% compared to the results of other studies(Lu et al., 2021; Zhang et al., 2013). Prior research has indicated that while micropores in GAC contribute to a larger specific surface area and higher adsorption capacity, larger pores can create more favorable conditions for microbial colonization (Andersson et al., 2001; Dong et al., 2019), potentially enhancing the biodegradation process; clearly, bacterial microbes are too large (~ > 0.2 μm) to enter the micro-, and meso-, pores. Therefore, the superior DOC removal performance of the C-GAC can be attributed to its rich macroporous distribution promotes the colonization of distinct microbial communities, which will be discussed in greater detail in the following sections. Interestingly, while the adsorption kinetics (Figure S4) indicated a lower capacity of C-GAC for adsorbing NOM from the water sample compared to B-GAC, C-GAC proved to be a more effective biofilter substrate (Figure 2A), yielding better effluent quality over extended operation. This phenomenon indicates that biodegradability, rather than intrinsic adsorption performance, is the critical factor for long-term operational effectiveness (225-257 days).

Figure 2

The analysis of EEM spectra through PARAFAC revealed that the water samples can be categorized into three distinct components: microbial humic-like (C1) (Dainard et al., 2019; Osburn et al., 2017), protein-like (C2) (Kida et al., 2019; Murphy et al., 2006), and tyrosine-like (C3) (Chen et al., 2017; Guéguen et al., 2014; Lin and Guo, 2020) components (Figure 2C). Pearson correlation analysis further revealed that DOM levels in the water samples were significantly positively correlated with C1 (Figure S7). Consequently, the C-GAC system achieved removal efficiencies of 80% for DOM and 99% for C1. In contrast, DOM removal efficiencies in both B-GAC and CS-GAC declined to approximately 60%, accompanied by a corresponding decrease in C1 removal rates. This effect was particularly pronounced in the middle and bottom segments. The C-GAC system demonstrated superior performance in removing the C1 component compared to the B-GAC and CS-GAC systems (Figure 2D). By utilizing SEC (Figure 2E), it was observed that all systems effectively removed NOM components across the full range of molecular weights when the HRT was relatively long (24 h). However, upon reducing the HRT to 6 h, the C-GAC system maintained a high level of NOM removal from raw water, while B-GAC and CS-GAC exhibited a decreased capability in this regard. Furthermore, results from FTIR analysis revealed a significantly greater reduction in -OH and -COOH groups in the sample from the top location of the C-GAC system compared to both B-GAC and CS-GAC (SI, Figure S8). Because physical and chemical adsorption dominated the overall adsorption process, rather than electrostatic attraction, the enhanced reduction can be attributed to the higher proportion of carboxyl groups on the C-GAC surface. These groups facilitate adsorption (Karanfil et al., 1999) and subsequent biodegradation of hydrophilic organic compounds (Grasset et al., 2023). In addition, the efficient degradation of hydrophilic organic compounds may be attributed to their own massive adsorption which affects the survival and reproduction of some strains and promotes the enrichment of some strains (preferring to degrade hydrophilic organic classes), which will be discussed in the microbiology section (Deng et al., 2020; Yu et al., 2020).

Molecular Transformation of NOM

The influence of different types of GAC on the removal of NOM was further examined at the molecular level using FT-ICR-MS (Figure 3). Based on the results from the previous section (DOC, EEM, and SEC), the C-GAC water sample, which demonstrated the best treatment performance, and the CS-GAC water sample, which showed the poorest performance, were selected for comparison. The analysis revealed that the samples from the top location from the C-GAC and CS-GAC systems contained 3932 and 5770 detected molecules, respectively, which is consistent with previous findings indicating that C-GAC outperformed CS-GAC in terms of NOM removal efficiency. These detected molecules can be categorized into seven groups: lignins, tannins, proteins, lipids, condensed aromatics, unsaturated hydrocarbons, and carbohydrates (Li et al., 2024; Lin et al., 2024). Compared to CS-GAC, C-GAC demonstrated a greater efficiency in removing relatively stable and biorefractory organic compounds (Hu et al., 2022b), such as lignin (2047 vs. 3528), tannins (614 vs. 1156), and condensed aromatics (149 vs. 364) (Figure 3B). Additionally, the NOSC and DBE values were lower in the top sample of the C-GAC system, while its AI_{mod} values approached zero, indicating that the sample contained lower levels of aromaticity and oxidized organic compounds (Figure 3C and D).

Regarding the m/z (mass-to-charge ratio) distribution, the top sample from the CS-GAC system exhibited a higher number of high m/z molecules in the condensed aromatic and lignin regions compared to the C-GAC system, while the latter displayed an increased abundance of molecules within the lipid and protein categories (Figure 3F). Furthermore, the C-GAC sample contained more aliphatic substances ($1.5 \leq H/C \leq 2.2$), believed to be generated via NOM biodegradation (Liu et al., 2023d; Ma et al., 2024), totalling 1144 compared to 793 in the CS-GAC sample (Figure 3E). This finding suggests that NOM degradation is more active in the C-GAC system. Moreover, it was observed that the top sample from the C-GAC contained significantly fewer organic molecules with nitrogen and sulfur elements compared to the CS-GAC system (1463

vs. 2174 for nitrogen, and 724 vs. 1623 for sulfur, respectively) (Figure S10). Among them, the N- and NS-containing compounds in C-GAC are primarily concentrated in lipids and proteinaceous materials (easily biodegradable), whereas those in CS-GAC are mainly found in tannins and lignin (difficult to biodegrade). It has been reported that nitrogen (N) can disrupt the competition between efficient and inefficient decomposers, leading to lignin accumulation through ammonia metabolite inhibition(FOG, 1988). This indicates that the microorganisms in the C-GAC system possess stronger degradation capabilities, demonstrating significant advantages in promoting the removal of nitrogen- and sulfur-containing compounds.

Figure 3

The characterizations of BAC particles

At the end of the experimental period, the electrochemical properties of the BAC granules were examined (Figures 4A-4D). The results from EIS revealed that the charge transfer resistance (R_{CT}) of the CS-GAC (1501 ± 28 ohms) was significantly higher than that of the C-GAC (1246 ± 37 ohms) and B-GAC (1232 ± 39 ohms). Additionally, CV measurements indicated that for the systems operated over a long period, the capacitance of the microbe-acclimated C-GAC was 1.32 and 1.92 times greater than that of the B-GAC and CS-GAC, respectively (Figure 4C). The slope of the CV curve was also indicative of the electrical resistance of the GAC, further supporting the finding that C-GAC exhibited the lowest resistivity. Lower resistances facilitate electron transfer among microbes on the surfaces of BAC granules, enhancing the biodegradation of NOM and, consequently, its removal efficiency (An et al., 2022). Furthermore, previous studies have indicated that a higher concentration of EPS could result in bacteria being enveloped, potentially hindering extracellular electron transfer (Liu et al., 2023b; Wang et al., 2021). Notably, the EPS content (comprising polysaccharides and proteins) on the surface of C-GAC was the lowest among the three types of GAC analyzed, measuring 3.10 ± 0.3 mg/g and 0.37 ± 0.0 mg/g for the two types of EPS. This result is consistent with the electrochemical properties of low resistance

and high electron transfer efficiency measured by C-GAC. Therefore, the long-term operated BAC system using C-GAC not only resulted in reduced electron transfer resistance, thus promoting the biodegradation of NOM, but also exhibited higher adsorption capabilities for NOM, further improving its removal efficiency. Additionally, an interesting phenomenon was observed: although EPS content on the C-GAC surface was low, microbial activity was high. This can be attributed to the favorable macroporous structure of C-GAC, which reduces the need for microorganisms to secrete EPS for attachment. Consistent with the electrochemical results, C-GAC creates a microenvironment with extremely low mass transfer resistance and high environmental stability, enabling microorganisms to maximize energy utilization for metabolism and growth, thereby exhibiting enhanced activity.

Figure 4

The impacts on microbial diversity

Bray-Curtis distance and principal co-ordinates analysis (PCoA) were employed to assess the community diversity of the three GAC systems operated over a long-term. As illustrated in Figure 5A, microbial populations in the C-GAC, B-GAC, and CS-GAC systems were distinctly separated along the first and second axes of the PCoA, indicating that the different types of GAC significantly influenced the microbial community structure (Adonis, $R^2 = 0.7797$, $P = 0.005$). The Simpson index further revealed significant differences in alpha diversity among the three systems, as evidenced by the Kruskal-Wallis test ($P < 0.05$) (Figure 5B). The Venn diagram analysis showed that the proportion of core shared microorganisms among the three systems was less than 30%, while the proportion of unique microorganisms in each system exceeded 50% (Figure 5C). Notably, the C-GAC system exhibited an enrichment of the genera *Desulfosporosinus* (8.67 ± 4.0%, versus 0% in B-GAC and 2.33 ± 1.5% in CS-GAC) and *Denitratisoma* (8.67 ± 0.6%, versus 4.67 ± 0.6% in B-GAC and 2.67 ± 0.6% in CS-GAC) (Figure 5D). These genera are associated with the biodegradation of humic acid, both artificial and natural organic matter, as well as the

417 removal of nitrate, nitrite, and sulfate salts (Choi et al., 2022; Fang et al., 2024; Liu et
418 al., 2023c; Villemur et al., 2006). *Desulfosporosinus* typically use sulfate as the
419 terminal electron acceptor in DOM degradation, and they can grow in a sulfate
420 dependent manner using hydrogen and various organic compounds. In addition,
421 unsaturated hydrocarbons (e.g., benzene, toluene, phenols) can be activated, then
422 converted by hydrolytic enzymes into straight-chain fatty acids. These are ultimately
423 oxidized to CO_2 or used in cellular synthesis, while simultaneously providing electrons
424 for sulfate reduction, consistent with the observed levels of unsaturated aromatic
425 hydrocarbons and sulfur-containing compounds in the FTICR data (Meckenstock et al.,
426 2016; Zhang et al., 2023). Furthermore, the relative abundance of the family
427 *Rhodocyclaceae* in the C-GAC system (29.1 ± 1.0%) was found to be more than double
428 that observed in both the B-GAC (13.9 ± 1.0%) and CS-GAC (14.4 ± 1.0%) systems
429 (Figure 5E). Based on the literature survey, it was synthesized that the family
430 *Rhodocyclaceae* is a species that prefers hydrophilic substances, which may be one of
431 the most important reasons for its enrichment in the C-GAC(Oren, 2014; Wang et al.,
432 2020). At the genus level (Figure S14), *unclassified_f__Rhodocyclaceae*,
433 *Denitratisoma* and *Sulfuritalea* as the main enriched species (belong to
434 Rhodocyclaceae). Compared to B-GAC (19 ± 1.0%, 29 ± 1.0%, 31 ± 1.0%) and CS-
435 GAC (14 ± 1.0%, 16 ± 1.0%, 56 ± 1.0%), of which the former two are more enriched
436 in the C-GAC (68 ± 1.0%, 55 ± 1.0%, 13 ± 1.0%). Previous studies have indicated that
437 the family *Rhodocyclaceae* possesses various metabolic functions, such as reducing
438 organic aromaticity, desulfurization, and denitrification (Corteselli et al., 2017; Smalley
439 et al., 2015), which can grow on selected monocyclic and polycyclic aromatic
440 compounds as the sole carbon source and use nitrate and ammonia as the nitrogen
441 source, contributing significantly to the biodegradation of NOM and the removal of
442 nitrogen-containing organic substances. It was also found to contribute significantly to
443 the degradation of unsaturated hydrocarbons, condensed aromatics and aliphatic
444 DOM(Chakraborty et al., 2005; Li et al., 2023; Rodrigues et al., 2019). Furthermore,
445 the genus *Rhodiola* is rich in dioxygenases and monooxygenases capable of ring-

446 opening degradation of aromatic compounds, aiding in the breakdown of aromatic
447 monomers (degradation products of lignin). This indicates its ability to directly
448 participate in downstream steps of the lignin degradation pathway (Chou et al., 2008),
449 consistent with the lignin removal observed in FTICR-MS.

450 **Figure 5**

451

452 **Synergistic effects on microbial interactions**

453 Co-occurrence network analysis at the genus level revealed interspecific interactions
454 among different microbial populations (Figure 6A-6C, Spearman's correlation
455 coefficient $r > 0.6$, $p < 0.05$). Compared to B-GAC (54.55%) and CS-GAC (57.76%),
456 the lowest positive correlation between microorganisms was found in the C-GAC
457 (52.70%) system, which suggests that the cooperation between microorganisms is
458 weaker than the former two, and also suggests that this system may rely on some
459 dominant strains to dominate DOM degradation. We found that the family
460 *Rhodocyclaceae* was the most enriched in the C-GAC system, and it had a good
461 degradation effect on difficult-to-biodegrade aromatic hydrocarbons (Táncsics et al.,
462 2023). In addition, we found that the family *Rhodocyclaceae* maintained a positive
463 correlation with other strains (Figure S15). There is a positive correlation between the
464 inclusion of the genera *Sulfuritalea* (belonging to the family *Rhodocyclaceae*) and the
465 genera *Desulfosnorosinus*, which are known to synergize in the degradation of
466 DOM(Woyke et al., 2006). In addition, there was also a positive correlation between
467 the genera *Azospira* (belonging to the family *Rhodococcaceae*) and the genera
468 *Pseudomonas.* They have been reported to synergistically degrade the aromatic
469 hydrocarbon DOM while accomplishing nitrogen removal(Chakraborty et al., 2005).
470 This also suggests that the family *Rhodophyceae* play an important role in synergizing
471 with other microbial denitrification to degrade aromatic compounds. It was also
472 confirmed that some of the dominant strains in the C-GAC system (like the family
473 *Rhodophyceae*) dominated the degradation of DOM, thus increasing the efficiency. The

C-GAC system exhibited the lowest average path length (2.74) compared to the B-GAC (4.19) and CS-GAC (3.60) systems, indicating a more compact network and stronger microbial interactions within the C-GAC system. Additionally, the higher average clustering coefficient for the C-GAC system (0.82) compared to the B-GAC (0.73) and CS-GAC (0.78) systems suggests that the dominant strains within the C-GAC system were more closely related to one another. Metabolic function predictions for microorganisms in the C-GAC system, generated by PICRUSt2, indicated that certain metabolic functions related to biodegradation (e.g., bacterial chemotaxis, propionate, and butanoate metabolism) were enhanced in this system compared to the other two (SI, Figure S11). These important metabolic functions enhance microbial activity in C-GAC and strengthen DOM metabolism. In contrast, both B-GAC and CS-GAC contained more amino acid degradation genes, indicating that they preferentially degrade labile DOM while leaving behind more recalcitrant DOM (Zhou et al., 2024). This also explains why C-GAC maintains more stable DOM removal from the perspective of microbial metabolism. Overall, the results suggest that the metabolic functions provided by microorganisms cannot simply be replaced by activated carbon adsorption; they play a crucial role in improving system performance.

Furthermore, a significant correlation was observed between microbial diversity and the physicochemical properties of GAC, particularly with respect to the distribution of mesoporous volume and the content of surface carboxyl group (Figure 6D). The properties of effluent NOM were also influenced by GAC's surface characteristics; specifically, the oxygen-containing functional groups on the GAC surface enhanced the adsorption of more hydrophilic NOM (Karanfil et al., 1999; Yoshida et al., 2013) and the pore size of GAC serves to selectively screen the size of the adsorbed NOM (Karanfil and Kilduff, 1999). Additionally, figure 6D revealed that the electrical resistance of GAC exhibits a negative correlation with the surface carboxyl group content, while showing a positive correlation with its phenolic hydroxyl group content. Further correlation analysis indicated that carboxyl groups have a stronger correlation

with GAC resistance than phenolic hydroxyl groups (Figure S12), indicating that carboxyl groups play a more critical role in influencing the electrical resistance of GAC. This result suggests that although phenolic hydroxyl groups also enhance hydrophilicity, the carboxyl group content represents the dominant factor influencing conductivity Moreover, a close relationship was identified between microbial diversity and the characteristics of the removed NOM, including its aromaticity (UV254), as well as the II, IV, and V regions of fluorescent substances (Figure 6E). This relationship implies that the different types of NOM adsorbed onto GAC can significantly affect the structure of microbial communities adapted to long-term operation in BAC systems.

Using PLS-PM (Figure 6F), it was determined that the carboxyl group on the surface of GAC can indirectly influence microbial community structure by affecting the electrical conductivity of the GAC (1.06). Surface carboxyl groups were found to enhance the electrical conductivity of GAC, facilitating electron transfer between microorganisms and promoting the enrichment of microbial species that favor hydrophilic DOM. Additionally, the pore size structure of GAC was shown to influence the microbial communities adapted to it, with mesopores favoring the enrichment of dominant microbes (0.40). The surface carboxylate content of GAC was more effective in influencing the dominant microbial strains than the pore size distribution, which is the same as the results of the previous study(Lu et al., 2021). Furthermore, the pore size of GAC affects the size of adsorbed NOM(Karanfil et al., 1999), while the carboxyl group on the GAC surface enhance the adsorption of hydrophilic organics, thereby indirectly influencing the enrichment of dominant microbes on the GAC surface (Hu et al., 2022a).

During long-term operation, GAC is transformed into BAC and becomes encapsulated by microbial EPS. The resistance of BAC is primarily dependent on the intrinsic resistance of the GAC (1.59) and varies with the colonizing microbial populations. The degradation of NOM is mainly influenced by microbial diversity and pore size distribution (0.61). High molecular weight NOM adsorbed on the surface of BAC is

gradually degraded and converted into low molecular weight organic substances, thereby restoring the adsorption capacity of the available sites for the further biodegradation of other organic compounds.

Figure 6

Conclusion

In this study, we systematically examined how variations in the surface functional group distribution of GAC influence microbial community formation on BAC filters and, consequently, the efficiency of NOM removal. The physicochemical properties of GAC directly shape microbial communities and indirectly affect dominant populations by altering the characteristics of adsorbed NOM. Results showed that C-GAC, with greater mesoporosity (1.87–2.30-fold higher) and surface –COOH concentration (1.69–3.06-fold higher), supported a distinct microbial community and achieved superior NOM removal (83.6 ± 1.4%)—approximately 20% higher than B-GAC and CS-GAC after 357 days. C-GAC enriched key microorganisms (e.g., *Desulfosporosinus*, *Denitratisoma*, and *Rhodocyclaceae*) associated with NOM metabolism, improving the removal of lignin, tannin, and condensed aromatic compounds by 42–59% compared to B-GAC. This improvement was attributed to the enrichment of dominant microbial populations, which not only enhanced interconnections among different species but also reduced average path lengths between them, thereby promoting a more efficient NOM degradation process. Furthermore, PLS-PM modeling revealed that –COOH groups had a stronger direct and indirect influence on microbial structure than pore size distribution, and that microbial structure and pore size distribution were the primary factors governing NOM degradation.

This study provides practical guidance for selecting BAC filter media and underscores the importance of both adsorbent properties and microbial ecology in optimizing long-term NOM removal from surface water. Further research is needed to clarify how characteristics of dissolved organic matter shape microbial diversity during biodegradation.

CRediT authorship contribution statement

Han Chen: Investigation, Writing – original draft; Junling Wang: Writing – review & editing; Lei Xu: Conceptualization, Supervision, Writing – original draft, review & editing; Peng Zhou: Investigation; Nigel J. D. Graham: Writing – review & editing; Wenzheng Yu: Supervision, Writing – review & editing, Resources, Funding acquisition.

Declaration of interests

The authors declare that they have no known competing financial interests or personal relationships that could have appeared to influence the work reported in this paper.

Data availability

Data will be made available on request.

Acknowledgments

This work was supported by the National Key Research and Development Program of China (Grant No. 2024YFD1700103), and the Beijing Natural Science Foundation (No. JQ21032).

Appendix A. Supplementary data

References

An, T., Chang, Y., Xie, J., Cao, Q., Liu, Y. and Chen, C. 2022. Deciphering physicochemical properties and enhanced microbial electron transfer capacity by magnetic biochar. Bioresour Technol 363(0960-8524), 127894.

Andersson, A., Laurent, P., Kihn, A., Prevost, M. and Servais, P. 2001. Impact of temperature on nitrification in biological activated carbon (BAC) filters used for drinking water treatment. Water Res 35(12), 2923-2934.

Antony, R., Willoughby, A.S., Grannas, A.M., Catanzano, V., Sleighter, R.L., Thamban, M., Hatcher, P.G. and Nair, S. 2017. Molecular Insights on Dissolved Organic Matter Transformation by Supraglacial Microbial Communities. Environ Sci Technol 51(8), 4328-4337.

Bianco, A., Deguillaume, L., Chaumerliac, N., Vaitilingom, M., Wang, M., Delort, A.M. and Bridoux, M.C. 2019. Effect of endogenous microbiota on the molecular composition of cloud water: a study by Fourier-transform ion cyclotron resonance mass spectrometry (FT-ICR MS). Sci Rep 9(1), 7663.

Blair, M.F., Vaidya, R., Salazar-Benites, G., Bott, C.B. and Pruden, A. 2024. Relating microbial community composition to treatment performance in an ozone-biologically active carbon filtration potable reuse treatment train. Water Res. 262, 122091.

Chakraborty, R., O'Connor Susan, M., Chan, E. and Coates John, D. 2005. Anaerobic Degradation of Benzene, Toluene, Ethylbenzene, and Xylene Compounds by Dechloromonas Strain RCB. Applied and Environmental Microbiology 71(12), 8649-8655.

Chen, M., Kim, S.H., Jung, H.J., Hyun, J.H., Choi, J.H., Lee, H.J., Huh, I.A. and Hur, J. 2017. Dynamics of dissolved organic matter in riverine sediments affected by weir impoundments: Production, benthic flux, and environmental implications. Water Res 121, 150-161.

Chen, S.Y., Gu, Y.Z., Liu, E.Y., Wu, M.H., Cheng, X.L., Yang, P.Z., Bahadur, A., Bai, R.Q., Chen, J.W., Zhang, M.Y., Wu, J.H. and Feng, Q. 2024. Freeze-thaw strength increases microbial stability to enhance diversity-soil multifunctionality relationship. Commun. Earth Environ. 5(1), 11.

Cheng, J., Bi, C., Zhou, X., Wu, D., Wang, D., Liu, C. and Cao, Z. 2023. Preparation of Bamboo-Based Activated Carbon via Steam Activation for Efficient Methylene Blue Dye Adsorption: Modeling and Mechanism Studies. Langmuir 39(39), 14119-14129.

Choi, B.Y., Park, J., Ham, B., Kirk, M.F. and Kwon, M.J. 2022. Effect of CO₂ on biogeochemical reactions and microbial community composition in bioreactors with deep groundwater and basalt. Sci. Total Environ. 807, 11.

Chou, J.H., Jiang, S.R., Cho, J.C., Song, J., Lin, M.C. and Chen, W.M. 2008. Azonexus hydrophilus sp. nov., a nifH gene-harbouring bacterium isolated from freshwater. Int J Syst Evol Microbiol 58(Pt 4), 946-951.

Christou, A., Beretsou, V.G., Iakovides, I.C., Karaolia, P., Michael, C., Benmarhnia, T., Chefetz, B., Donner, E., Gawlik, B.M., Lee, Y., Lim, T.T., Lundy, L., Maffettone, R.,

Rizzo, L., Topp, E. and Fatta-Kassinos, D. 2024. Sustainable wastewater reuse for agriculture. Nat. Rev. Earth Environ. 5(7), 504-521.

Cordero-Lanzac, T., Rosas, J.M., García-Mateos, F.J., Ternero-Hidalgo, J.J., Palomo, J., Rodríguez-Mirasol, J. and Cordero, T. 2018. Role of different nitrogen functionalities on the electrochemical performance of activated carbons. Carbon 126, 65-76.

Corteselli, E.M., Aitken, M.D. and Singleton, D.R. 2017. Rugosibacter aromaticivorans gen. nov., sp. nov., a bacterium within the family Rhodocyclaceae, isolated from contaminated soil, capable of degrading aromatic compounds. Int J Syst Evol Microbiol 67(2), 311-318.

D'Abzac, P., Bordas, F., Van Hullebusch, E., Lens, P.N. and Guibaud, G. 2010. Extraction of extracellular polymeric substances (EPS) from anaerobic granular sludges: comparison of chemical and physical extraction protocols. Appl Microbiol Biotechnol 85(5), 1589-1599.

Dainard, P.G., Guéguen, C., Yamamoto-Kawai, M., Williams, W.J. and Hutchings, J.K. 2019. Interannual Variability in the Absorption and Fluorescence Characteristics of Dissolved Organic Matter in the Canada Basin Polar Mixed Waters. Journal of Geophysical Research: Oceans 124(7), 5258-5269.

Dal Bello, M., Lee, H., Goyal, A. and Gore, J. 2021. Author Correction: Resource-diversity relationships in bacterial communities reflect the network structure of microbial metabolism. Nat Ecol Evol 5(10), 1463.

Deng, S., Zheng, X., Chen, X., Zheng, S., He, X., Ge, T., Kuzyakov, Y., Wu, J., Su, Y. and Hu, Y. 2020. Divergent mineralization of hydrophilic and hydrophobic organic substrates and their priming effect in soils depending on their preferential utilization by bacteria and fungi. Biol. Fertil. Soils 57(1), 65-76.

Dong, L., Liu, W., Yu, Y., Hou, L., Gu, P. and Chen, G. 2019. Preparation, characterization, and application of macroporous activated carbon (MAC) suitable for the BAC water treatment process. Sci Total Environ 647, 1359-1367.

Fang, S., Geng, Y., Wang, L., Zeng, J., Zhang, S., Wu, Y. and Lin, X. 2024. Coupling between 2, 2′, 4, 4′-tetrabromodiphenyl ether (BDE-47) debromination and methanogenesis in anaerobic soil microcosms. Sci. Total Environ. 914, 169831.

FOG, K. 1988. The effect of added nitrogen on the rate of decomposition of organic matter. Biological Reviews 63(3), 433-462.

Gerrity, D., Arnold, M., Dickenson, E., Moser, D., Sackett, J.D. and Wert, E.C. 2018. Microbial community characterization of ozone-biofiltration systems in drinking water and potable reuse applications. Water Res. 135, 207-219.

Goertzen, S.L., Thériault, K.D., Oickle, A.M., Tarasuk, A.C. and Andreas, H.A. 2010. Standardization of the Boehm titration. Part I. CO2 expulsion and endpoint determination. Carbon 48(4), 1252-1261.

Grasset, C., Groeneveld, M., Tranvik, L.J., Robertson, L.P. and Hawkes, J.A. 2023. Hydrophilic Species Are the Most Biodegradable Components of Freshwater Dissolved Organic Matter. Environ Sci Technol 57(36), 13463-13472.

Gryglewicz, G., Machnikowski, J., Lorenc-Grabowska, E., Lota, G. and Frackowiak, E. 2005. Effect of pore size distribution of coal-based activated carbons on double layer capacitance. Electrochimica Acta 50(5), 1197-1206.

Guéguen, C., Cuss, C.W., Cassels, C.J. and Carmack, E.C. 2014. Absorption and fluorescence of dissolved organic matter in the waters of the Canadian Arctic Archipelago, Baffin Bay, and the Labrador Sea. Journal of Geophysical Research: Oceans 119(3), 2034-2047.

Han, L., Liu, W., Chen, M., Zhang, M., Liu, S., Sun, R. and Fei, X. 2013. Comparison of NOM removal and microbial properties in up-flow/down-flow BAC filter. Water Res 47(14), 4861-4868.

Hashim, D.S.B., Liew, J.Y., Boon, J.G. and Ch'ng, H.Y. 2022. Multipurpose applications of bamboo as an activated carbon: An overview. Journal of Applied and Natural Science 14(2), 522-530.

Hu, A., Choi, M., Tanentzap, A.J., Liu, J., Jang, K.S., Lennon, J.T., Liu, Y., Soininen, J., Lu, X., Zhang, Y., Shen, J. and Wang, J. 2022a. Ecological networks of dissolved organic matter and microorganisms under global change. Nat Commun 13(1), 3600.

Hu, A., Jang, K.S., Meng, F., Stegen, J., Tanentzap, A.J., Choi, M., Lennon, J.T., Soininen, J. and Wang, J. 2022b. Microbial and Environmental Processes Shape the Link between Organic Matter Functional Traits and Composition. Environ Sci Technol 56(14), 10504-10516.

Huang, F., Graham, N.J.D., Su, Z., Xu, L. and Yu, W. 2024. Capabilities of Microbial Consortia from Disparate Environment Matrices in the Decomposition of Nature Organic Matter by Biofiltration. Water Res 262, 122047.

Huang, G., Geng, Q., Kang, W., Liu, Y., Li, Y., Xing, B., Liu, Q. and Zhang, C. 2019. Hierarchical porous carbon with optimized mesopore structure and nitrogen doping for supercapacitor electrodes. Microporous and Mesoporous Materials 288, 109576.

Jones, E.R., Bierkens, M.F.P. and van Vliet, M.T.H. 2024. Current and future global water scarcity intensifies when accounting for surface water quality. Nat. Clim. Chang. 14(6), 629-635.

Karanfil, T. and Kilduff, J.E. 1999. Role of Granular Activated Carbon Surface Chemistry on the Adsorption of Organic Compounds. 1. Priority Pollutants. Environ Sci Technol 33(18), 3217-3224.

Karanfil, T., Kilduff, J.E., Schlautman, M.A. and Weber, W.J. 1996. Adsorption of Organic Macromolecules by Granular Activated Carbon. 1. Influence of Molecular Properties Under Anoxic Solution Conditions. Environ Sci Technol 30(7), 2187-2194.

Karanfil, T., Kitis, M., Kilduff, J.E. and Wigton, A. 1999. Role of Granular Activated Carbon Surface Chemistry on the Adsorption of Organic Compounds. 2. Natural Organic Matter. Environ Sci Technol 33(18), 3225-3233.

Kida, M., Kojima, T., Tanabe, Y., Hayashi, K., Kudoh, S., Maie, N. and Fujitake, N. 2019. Origin, distributions, and environmental significance of ubiquitous humic-like fluorophores in Antarctic lakes and streams. Water Res 163, 114901.

Kim, B.C., Kim, Y.H. and Yamamoto, T. 2009. Adsorption characteristics of bamboo activated carbon. Korean J. Chem. Eng. 25(5), 1140-1144.

Li, M., Li, Z., Fu, L., Deng, L. and Wu, C. 2024. Molecular-level insights into dissolved organic matter and its variations of the full-scale processes in a typical petrochemical wastewater treatment plant. Water Res 261, 121990.

Li, S., Tan, X., Li, H., Gao, Y., Wang, Q., Li, G. and Guo, M.J.S.R. 2022. Investigation on pore structure regulation of activated carbon derived from sargassum and its application in supercapacitor. 12(1), 10106.

Li, X., Li, X., Li, C., Li, N., Zou, P., Gao, X. and Cao, Q. 2023. Nitrogen removal performances and metabolic mechanisms of denitrification systems using different volatile fatty acids as external carbon sources. Chem. Eng. J. 474, 145998.

Lin, B., An, X., Zhao, C., Gao, Y., Liu, Y., Qiu, B., Qi, F. and Sun, D. 2024. Analysis of urban composite non-point source pollution characteristics and its contribution to river DOM based on EEMs and FT-ICR MS. Water Res 266, 122406.

Lin, H. and Guo, L. 2020. Variations in Colloidal DOM Composition with Molecular Weight within Individual Water Samples as Characterized by Flow Field-Flow Fractionation and EEM-PARAFAC Analysis. Environ Sci Technol 54(3), 1657-1667.

Liu, M., Graham, N., Xu, L., Zhang, K. and Yu, W. 2023a. Bubbleless aerated-biological activated carbon as a superior process for drinking water treatment in rural areas. Water Res 240, 120089.

Liu, M., Graham, N.J.D., Xu, L., Zhang, K. and Yu, W. 2023b. Bubbleless Air Shapes Biofilms and Facilitates Natural Organic Matter Transformation in Biological Activated Carbon. Environ Sci Technol 57(11), 4543-4555.

Liu, Z., Yang, R., Zhang, D., Wang, J., Gao, M., Zhang, A., Liu, W. and Liu, Y. 2023c. Insight into the effect of particulate organic matter on sludge granulation at the low organic load: Sludge characteristics, extracellular polymeric substances and microbial communities response. Bioresour Technol 388, 129791.

Liu, Z., Yang, R.S., Zhang, D., Wang, J.X., Gao, M., Zhang, A.N., Liu, W.L. and Liu, Y.J. 2023d. Insight into the effect of particulate organic matter on sludge granulation at the low organic load: Sludge characteristics, extracellular polymeric substances and microbial communities response. Bioresour. Technol. 388, 10.

Lu, Z., Jing, Z., Huang, J., Ke, Y., Li, C., Zhao, Z., Ao, X. and Sun, W. 2022. Can we shape microbial communities to enhance biological activated carbon filter performance? Water Res 212, 118104.

Lu, Z., Li, C., Jing, Z., Ao, X., Chen, Z. and Sun, W. 2021. Implication on selection and replacement of granular activated carbon used in biologically activated carbon filters through meta-omics analysis. Water Res. 198, 117152.

Ma, K., Li, Y.Y., Song, W., Zhou, J.Y., Liu, X., Wang, M.Q., Gong, X.F., Wang, L.L. and Tu, Q.C. 2024. Disentangling drivers of mudflat intertidal DOM chemodiversity using ecological models. Nature Communications 15(1), 13.

Meckenstock, R.U., Boll, M., Mouttaki, H., Koelschbach, J.S., Cunha Tarouco, P., Weyrauch, P., Dong, X. and Himmelberg, A.M. 2016. Anaerobic Degradation of Benzene and Polycyclic Aromatic Hydrocarbons. Journal of molecular microbiology and biotechnology 26(1-3), 92-118.

Murphy, K.R., Ruiz, G.M., Dunsmuir, W.T. and Waite, T.D. 2006. Optimized parameters for fluorescence-based verification of ballast water exchange by ships. Environ Sci Technol 40(7), 2357-2362.

Nyika, J. and Dinka, M. 2022. Activated bamboo charcoal in water treatment: A mini-review. Materials Today: Proceedings 56, 1904-1907.

Oh, S., Hammes, F. and Liu, W.T. 2018. Metagenomic characterization of biofilter microbial communities in a full-scale drinking water treatment plant. Water Res 128, 278-285.

Oickle, A.M., Goertzen, S.L., Hopper, K.R., Abdalla, Y.O. and Andreas, H.A. 2010. Standardization of the Boehm titration: Part II. Method of agitation, effect of filtering and dilute titrant. Carbon 48(12), 3313-3322.

Oren, A. (2014) The Prokaryotes: Alphaproteobacteria and Betaproteobacteria. Rosenberg, E., DeLong, E.F., Lory, S., Stackebrandt, E. and Thompson, F. (eds), pp. 975-998, Springer Berlin Heidelberg, Berlin, Heidelberg.

Osburn, C.L., Anderson, N.J., Stedmon, C.A., Giles, M.E., Whiteford, E.J., McGenity, T.J., Dumbrell, A.J. and Underwood, G.J.C. 2017. Shifts in the Source and Composition of Dissolved Organic Matter in Southwest Greenland Lakes Along a Regional Hydro-climatic Gradient. Journal of Geophysical Research: Biogeosciences 122(12), 3431-3445.

Rodrigues, C., Núñez-Gómez, D., Silveira, D.D., Lapolli, F.R. and Lobo-Recio, M.A. 2019. Chitin as a substrate for the biostimulation of sulfate-reducing bacteria in the treatment of mine-impacted water (MIW). Journal of Hazardous Materials 375, 330-338.

Shah, A.A., Walia, S. and Kazemian, H. 2024. Electrolysis for ammonia removal and hydrogen generation in urban wastewater: Innovative approaches to the water crisis. J. Environ. Chem. Eng. 12(6), 8.

Siembida-Losch, B., Anderson, W.B., Wang, Y.M., Bonsteel, J. and Huck, P.M. 2015. Effect of ozone on biopolymers in biofiltration and ultrafiltration processes. Water Res 70, 224-234.

Smalley, N.E., Taipale, S., De Marco, P., Doronina, N.V., Kyrpides, N., Shapiro, N., Woyke, T. and Kalyuzhnaya, M.G. 2015. Functional and genomic diversity of methylotrophic Rhodocyclaceae: description of Methyloversatilis discipulorum sp. nov. Int J Syst Evol Microbiol 65(7), 2227-2233.

Táncsics, A., Banerjee, S., Soares, A., Bedics, A. and Kriszt, B. 2023. Combined Omics Approach Reveals Key Differences between Aerobic and Microaerobic Xylene-Degrading Enrichment Bacterial Communities: Rhodoferax—A Hitherto Unknown Player Emerges from the Microbial Dark Matter. Environmental Science & Technology 57(7), 2846-2855.

Villemur, R., Lanthier, M., Beaudet, R. and Lepine, F. 2006. The Desulfitobacterium genus. FEMS Microbiol Rev 30(5), 706-733.

Wagg, C., Schlaeppi, K., Banerjee, S., Kuramae, E.E. and van der Heijden, M.G.A. 2019. Fungal-bacterial diversity and microbiome complexity predict ecosystem functioning. Nat Commun 10(1), 4841.

Wang, H., Zheng, Y., Zhu, B. and Zhao, F. 2021. In situ role of extracellular polymeric substances in microbial electron transfer by Methylomonas sp. LW13. Fundamental Research 1(6), 735-741.

Wang, J.Z., Summers, R.S. and Miltner, R.J. 1995. Biofiltration performance: part 1, relationship to biomass. Journal AWWA 87(12), 55-63.

Wang, M., Bodirsky, B.L., Rijneveld, R., Beier, F., Bak, M.P., Batool, M., Droppers, B., Popp, A., van Vliet, M.T.H. and Strokal, M. 2024. A triple increase in global river basins with water scarcity due to future pollution. Nat. Commun. 15(1), 880.

Wang, X., Zhang, Q., Zhang, Z., Li, W., Liu, W., Xiao, N., Liu, H., Wang, L., Li, Z., Ma, J., Liu, Q., Ren, C., Yang, G., Zhong, Z. and Han, X. 2023. Decreased soil multifunctionality is associated with altered microbial network properties under precipitation reduction in a semiarid grassland. iMeta 2(2), e106.

Wang, Z., Li, W., Li, H., Zheng, W. and Guo, F. 2020. Phylogenomics of Rhodocyclales and its distribution in wastewater treatment systems. Scientific Reports 10(1), 3883.

Woyke, T., Teeling, H., Ivanova, N.N., Huntemann, M., Richter, M., Gloeckner, F.O., Boffelli, D., Anderson, I.J., Barry, K.W., Shapiro, H.J., Szeto, E., Kyrpides, N.C., Mussmann, M., Amann, R., Bergin, C., Ruehland, C., Rubin, E.M. and Dubilier, N. 2006. Symbiosis insights through metagenomic analysis of a microbial consortium. Nature 443(7114), 950-955.

Xu, L., Song, S., Graham, N.J.D. and Yu, W. 2024. Simultaneous removal of NOM and sulfate in a bioelectrochemical integrated biofilter treating reclaimed water. Water Res 252, 121193.

Yoshida, H., Amano, Y., Bizley, T., Fotoohi, B., Mercier, L. and Machida, M. 2013. Aromatic compound adsorption from aqueous solution on activated carbons: Effects of adsorbate polarity and surface functional groups. Carbon 60, 567.

Yu, M., Liu, S., Li, G., Zhang, H., Xi, B., Tian, Z., Zhang, Y. and He, X. 2020. Municipal wastewater effluent influences dissolved organic matter quality and microbial community composition in an urbanized stream. Sci Total Environ 705, 135952.

Yuksel, R. and Karakehya, N. 2024. High energy density biomass-derived activated carbon materials for sustainable energy storage. Carbon 221, 10.

Zhai, Y., Dou, Y., Zhao, D., Fulvio, P.F., Mayes, R.T. and Dai, S. 2011. Carbon materials for chemical capacitive energy storage. Adv Mater 23(42), 4828-4850.

Zhang, D.-Y., Li, W.-G., Gong, H.-N., Zhang, L., Gong, X.-J. and Liu, B.-Y. 2013. Evaluation of long term stability of seeded bacteria in a bio-enhanced activated carbon filter used for treating drinking water. International Biodeterioration Biodegradation 85, 701-708.

Zhang, Z., Sun, J., Gong, X., Wang, C. and Wang, H. 2023. Anaerobic biodegradation of pyrene and benzo[a]pyrene by a new sulfate-reducing Desulforamulus aquiferis strain DSA. Journal of Hazardous Materials 459, 132053.

Zhou, P., Tian, L., Siddique, M.S., Song, S., Graham, N.J.D., Zhu, Y.G. and Yu, W. 2024. Divergent Fate and Roles of Dissolved Organic Matter from Spatially Varied Grassland Soils in China During Long-Term Biogeochemical Processes. Environ Sci Technol 58(2), 1164-1176.

Figure Captions

Figure 1. The physical and surface chemical properties of three types of GAC: (A) The distribution of micropore and mesopore specific surface area and pore volume in the GACs; (B) The resistivity of the GACs; (C) The distribution of pore volume and specific surface area of micropores and mesopores in the GACs; (D) The concentration and distribution of surface acidic groups in the GACs; (E) High-resolution XPS spectra (C1s, O1s and N1s) of the GACs.

Figure 2. Differences in the removal of DOM by the three BAC systems: (A) The variation in concentration of DOC in the solution from the top location (middle, and bottom locations given in SI, Figure S3) of the different systems with operation time; (B) A differential analysis of UV_{254} and DOC concentrations in the top location of the three systems (Wilcoxon test); (C) The main fluorescent components common to all systems identified through PARAFAC analysis; (D) The removal rates for three types of fluorescent components (C1, C2, and C3) in various locations (top, mid, and bottom) of the three systems, throughout the entire operational process; (E) The molecular weight distribution of samples from the top location characterized at different HRTs (24 h, 12 h, and 6 h) (***, $p < 0.001$; **, $p < 0.01$; *, $p < 0.05$; ns, $p > 0.05$).

Figure 3. The molecular structure and properties of DOM in the samples from the C-GAC and CS-GAC systems: (A) The Van Krevelen diagram illustrates the unique molecular formulas; (B) The molecular number distribution of different compounds in the samples; (C) and (D) show the differences in the nominal oxidation state of carbon (NOSC), double bond equivalence (DBE), and modified aromaticity index (AI_{mod}) among the unique formulas; (E) The content of aliphatic compounds; (F) The Van Krevelen diagrams presenting the unique molecular formulas, with colors representing the m/z ratios of the molecules.

Figure 4. The electrochemical characteristics of BAC granules: (A) The EIS curves for the three GAC systems. (B) The resistance of GAC in the three systems (Wilcoxon test). (C) CV measurements for the GAC from the three systems. (D) The distribution of slopes from the CV curves is presented, indicating variations in charge transfer kinetics among the systems. (F, G) The content of polysaccharides and proteins in the BAC particles (***, $p < 0.001$; **, $p < 0.01$; *, $p < 0.05$; ns, $p > 0.05$).

Figure 5. The structure of the microbial population influenced by various environmental factors: (A) PCoA analysis based on Bray-Curtis distance; (B) Differences in microbial alpha diversity (Kruskal-Wallis test); (C) Venn diagrams

depicting the uniqueness of bacterial ASVs across the three GAC systems; (D) Histogram of LDA scores revealing bacterial genera exhibiting significant differences in abundance among the three GAC systems; (E) The distribution ratios of various microbial species across the different GAC systems at the family level (***, $p < 0.001$; **, $p < 0.01$; *, $p < 0.05$; ns, $p > 0.05$).

Figure 6. The co-occurrence network diagrams illustrate the relationships among microorganisms at the genus level for the three systems: C-GAC (A), B-GAC (B), and CS-GAC (C) (Red represents positive correlations, while gray indicates negative correlations, with colors corresponding to their respective genus); (D) The relationship between microbial composition and the characteristics of DOM, and the properties of GAC or BAC; (E) The impact of DOM characteristics on microbial composition; (F) PLS-PM analysis indicating that pore size distribution and the content of surface chemical groups in GAC significantly govern microbial diversity, either directly or indirectly, leading to different DOM removal efficiencies. In the PLS-PM model, red lines signify positive correlations while blue lines denote negative correlations, and the thickness of the lines is proportional to the magnitude of the correlation, with thicker lines representing greater contributions. The black line reflects aspects not directly related to the PLS-PM model but is part of the overall mechanism for DOM degradation (***, $p < 0.001$; **, $p < 0.01$; *, $p < 0.05$; ns, $p > 0.05$).

Figure 1

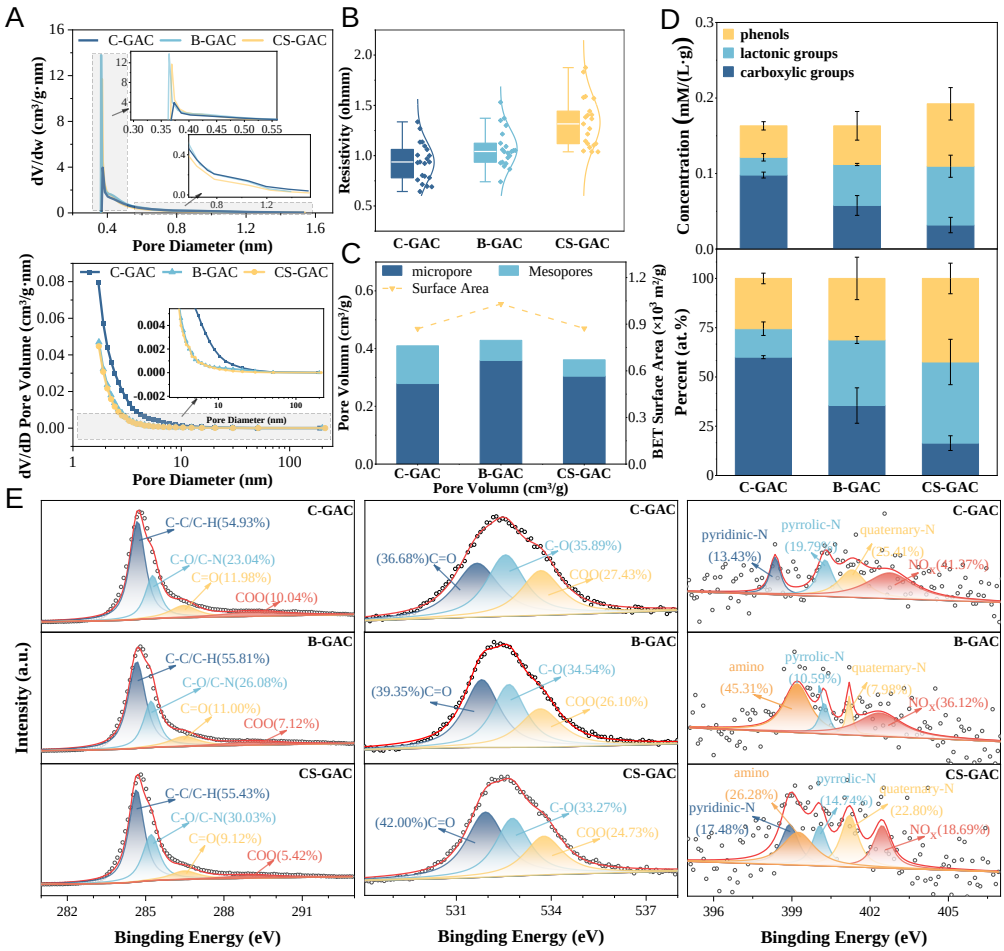

Figure 1. The physical and surface chemical properties of three types of GAC: (A) The distribution of micropore and mesopore specific surface area and pore volume in the GACs; (B) The resistivity of the GACs; (C) The distribution of pore volume and specific surface area of micropores and mesopores in the GACs; (D) The concentration and distribution of surface hydrophilic groups in the GACs; (E) High-resolution XPS spectra (C1s, O1s and N1s) of the GACs.

Figure 2

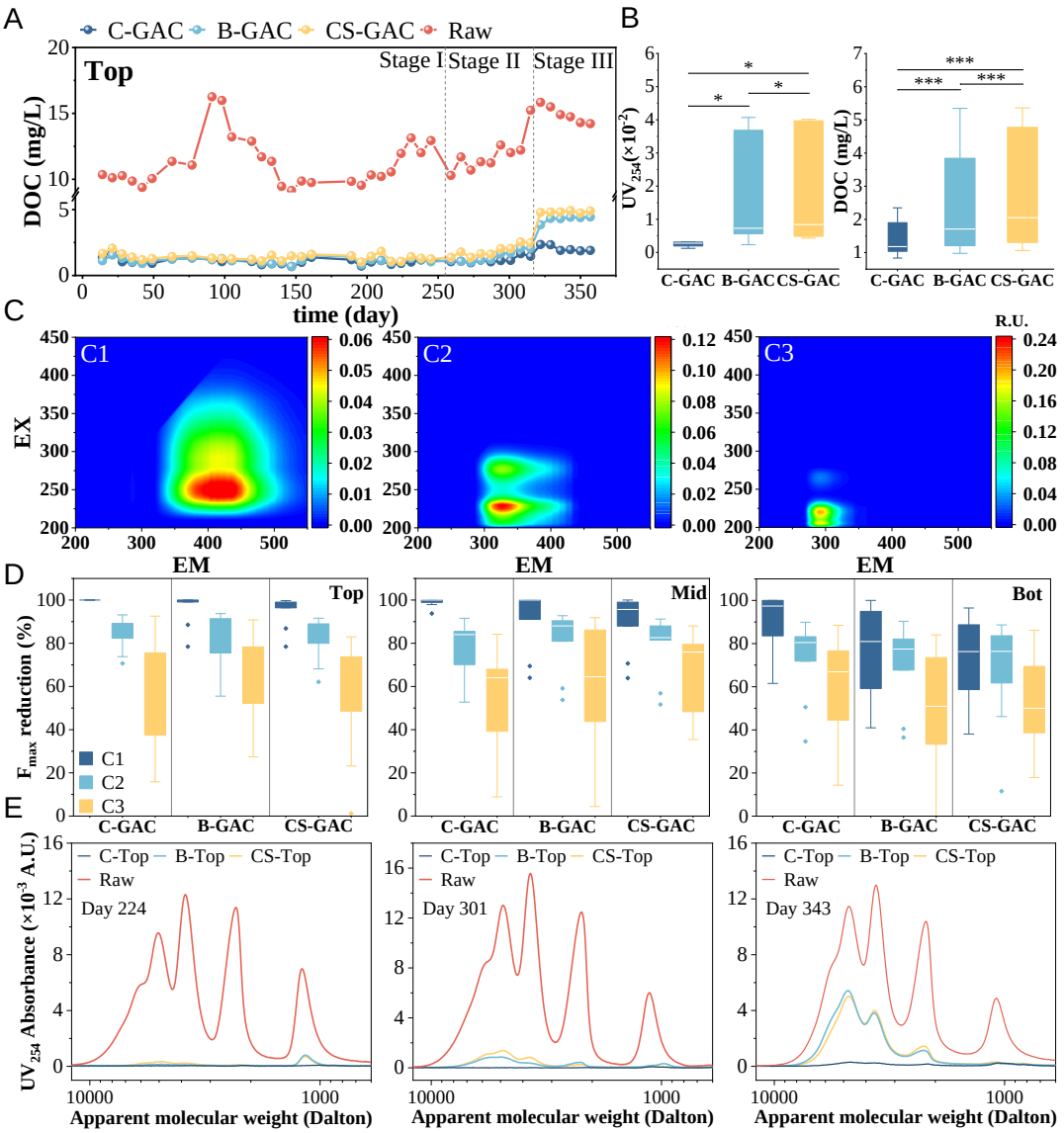

Figure 2. Differences in the removal of DOM by the three BAC systems: (A) The variation in concentration of DOC in the solution from the top location (middle, and bottom locations given in SI, Figure S3) of the different systems with operation time; (B) A differential analysis of UV_{254} and DOC concentrations in the top location of the three systems (Wilcoxon test); (C) The main fluorescent components common to all systems identified through PARAFAC analysis; (D) The removal rates for three types of fluorescent components (C1, C2, and C3) in various locations (top, mid, and bottom) of the three systems, throughout the entire operational process; (E) The molecular weight distribution of samples from the top location characterized at different HRTs (24 h, 12 h, and 6 h) (***, $p < 0.001$; **, $p < 0.01$; *, $p < 0.05$; ns, $p > 0.05$).

Figure 3

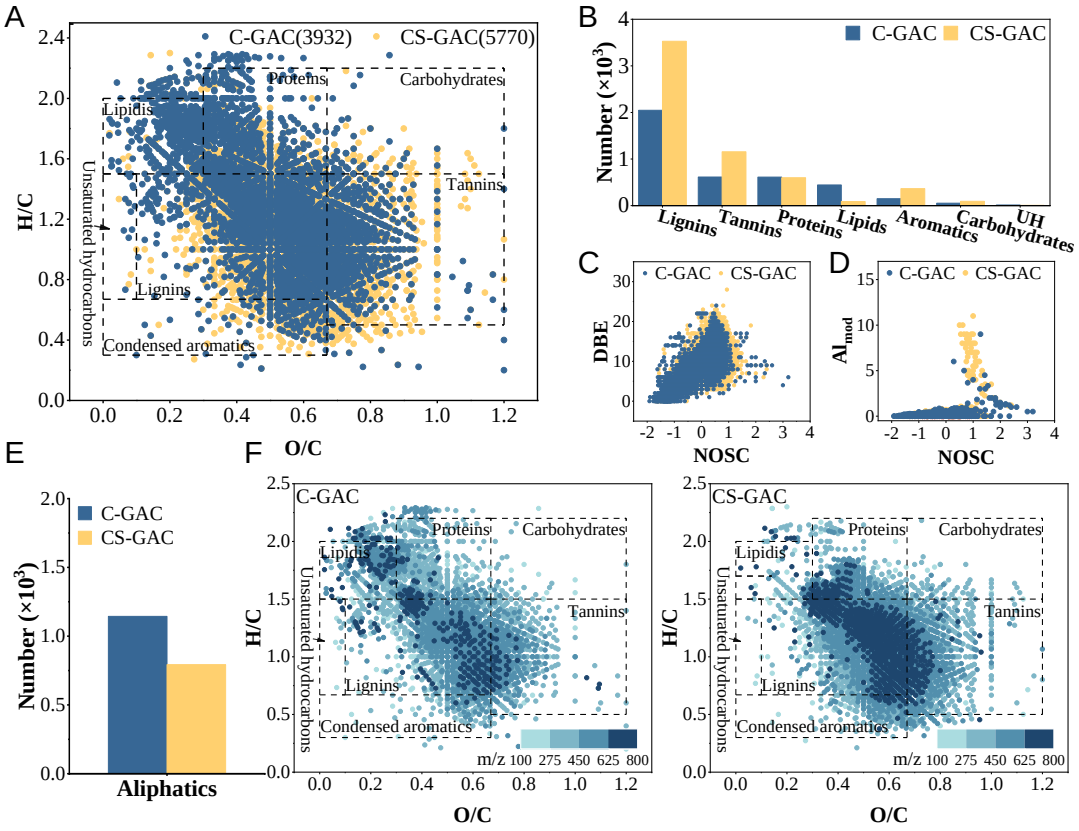

Figure 3. The molecular structure and properties of DOM in the samples from the C-GAC and CS-GAC systems: (A) The Van Krevelen diagram illustrates the unique molecular formulas; (B) The molecular number distribution of different compounds in the samples; (C) and (D) show the differences in the nominal oxidation state of carbon (NOSC), double bond equivalence (DBE), and modified aromaticity index (AI_{mod}) among the unique formulas; (E) The content of aliphatic compounds; (F) The Van Krevelen diagrams presenting the unique molecular formulas, with colors representing the m/z ratios of the molecules.

Figure 4

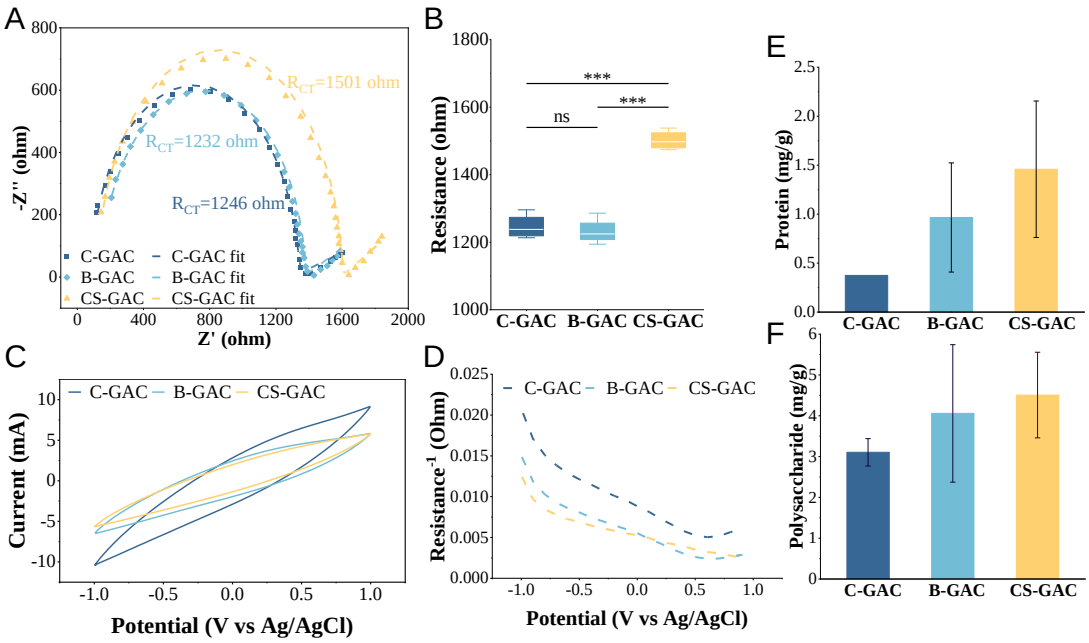

Figure 4. The electrochemical characteristics of BAC granules: (A) The EIS curves for the three GAC systems. (B) The resistance of GAC in the three systems (Wilcoxon test). (C) CV measurements for the GAC from the three systems. (D) The distribution of slopes from the CV curves is presented, indicating variations in charge transfer kinetics among the systems. (F, G) The content of polysaccharides and proteins in the BAC particles (***, $p < 0.001$; **, $p < 0.01$; *, $p < 0.05$; ns, $p > 0.05$).

Figure 5

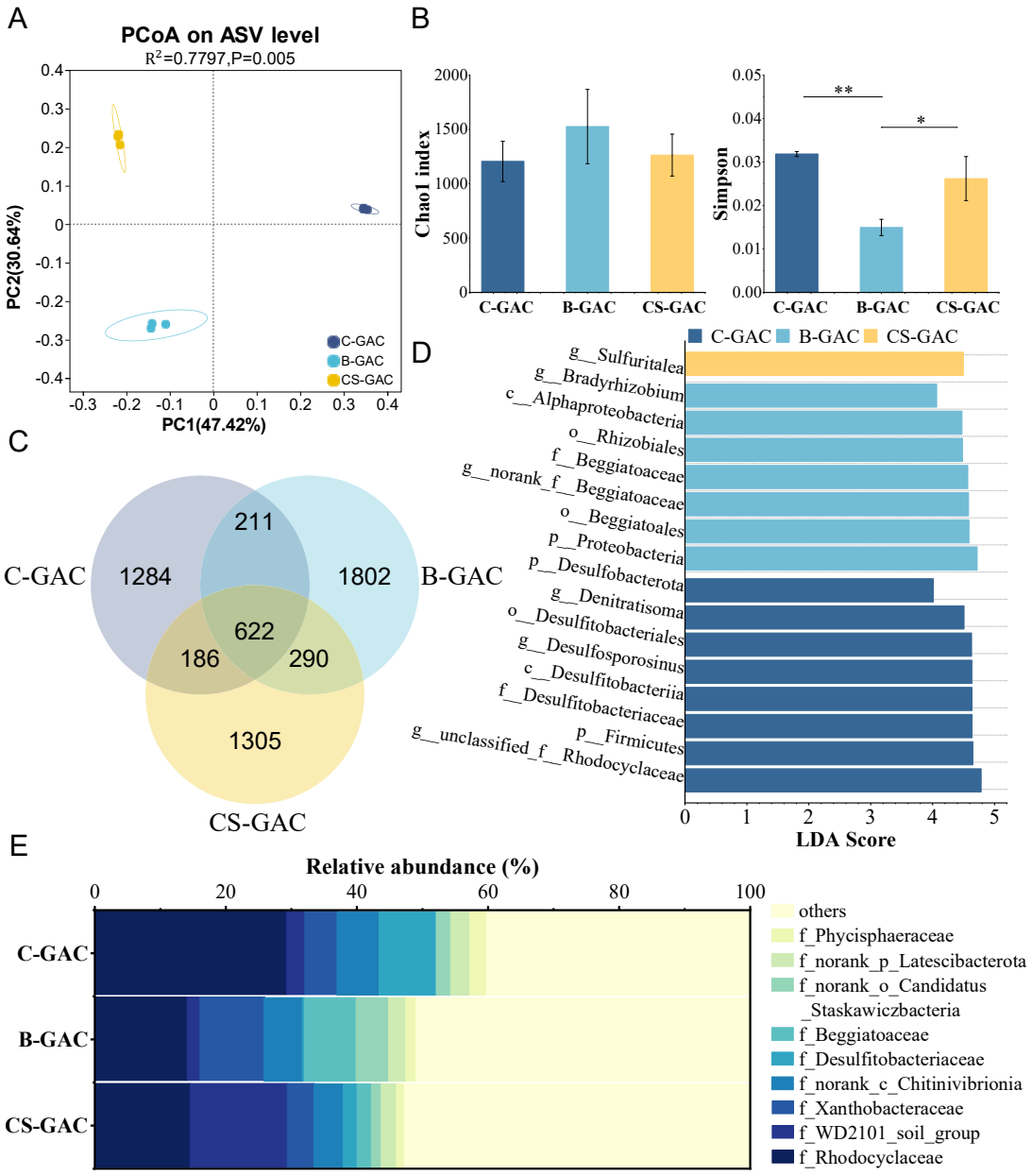

Figure 5. The structure of the microbial population influenced by various environmental factors: (A) PCoA analysis based on Bray-Curtis distance; (B) Differences in microbial alpha diversity (Kruskal-Wallis test); (C) Venn diagrams depicting the uniqueness of bacterial ASVs across the three GAC systems; (D) Histogram of LDA scores revealing bacterial genera exhibiting significant differences in abundance among the three GAC systems; (E) The distribution ratios of various microbial species across the different GAC systems at the family level (***, $p < 0.001$; **, $p < 0.01$; *, $p < 0.05$; ns, $p > 0.05$).

Figure 6

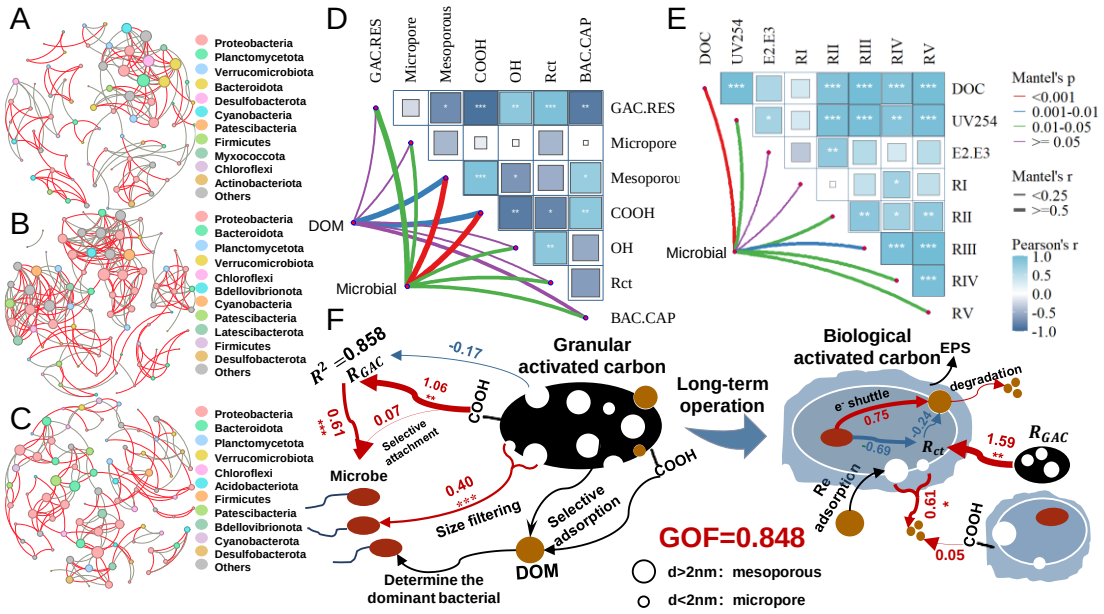

Figure 6. The co-occurrence network diagrams illustrate the relationships among microorganisms at the genus level for the three systems: C-GAC (A), B-GAC (B), and CS-GAC (C) (Red represents positive correlations, while gray indicates negative correlations, with colors corresponding to their respective genus); (D) The relationship between microbial composition and the characteristics of DOM, and the properties of GAC or BAC; (E) The impact of DOM characteristics on microbial composition; (F) PLS-PM analysis indicating that pore size distribution and the content of surface chemical groups in GAC significantly govern microbial diversity, either directly or indirectly, leading to different DOM removal efficiencies. In the PLS-PM model, red lines signify positive correlations while blue lines denote negative correlations, and the thickness of the lines is proportional to the magnitude of the correlation, with thicker lines representing greater contributions. The black line reflects aspects not directly related to the PLS-PM model but is part of the overall mechanism for DOM degradation (***, $p < 0.001$; **, $p < 0.01$; *, $p < 0.05$; ns, $p > 0.05$).